
Online spatio-temporal learning in deep neural networks

Thomas Bohnstingl*

IBM Research – Zurich
Institute of Theoretical Computer Science
Graz University of Technology

Stanisław Woźniak

IBM Research – Zurich

Wolfgang Maass

Institute of Theoretical Computer Science
Graz University of Technology

Angeliki Pantazi

IBM Research – Zurich

Evangelos Eleftheriou

IBM Research – Zurich

Abstract

Biological neural networks are equipped with an inherent capability to continuously adapt through online learning. This aspect remains in stark contrast to learning with error backpropagation through time (BPTT) applied to recurrent neural networks (RNNs), or recently even to biologically-inspired spiking neural networks (SNNs), because the unrolling through time of BPTT leads to system-locking problems. Online learning has recently regained the attention of the research community, focusing either on approaches that approximate BPTT or on biologically-plausible schemes applied in SNNs. Here we present an alternative perspective that is based on a clear separation of spatial and temporal gradient components. Combined with insights from biology, we derive from first principles a novel online learning algorithm, called online spatio-temporal learning (OSTL), which is gradient-equivalent to BPTT for shallow networks. We apply OSTL to SNNs allowing them for the first time to be trained online with BPTT-equivalent gradients. In addition, the proposed formulation uncovers a class of SNN architectures trainable online at low complexity. Moreover, we extend OSTL to deep networks while maintaining its key characteristics. Besides SNNs, the generic form of OSTL is applicable to a wide range of network architectures, including networks comprising long short-term memory (LSTM) and gated recurrent units (GRU). We demonstrate the operation of our algorithm on various tasks from language modelling to speech recognition, and obtain results on par with the BPTT baselines. The proposed algorithm provides a framework for developing succinct and efficient online training approaches for SNNs and in general deep RNNs.

1 Introduction

The brain has the unique capability to adapt to changing environment conditions through online learning in plastic synapses Kolb and Whishaw [1998] and is able to perform intelligent tasks still far out of reach of computers, while consuming very little amount of power Mead [1990]. Brain-inspired concepts in machine learning applications have so far primarily focused on incorporating the layered, highly interconnected topology of the biological neural networks in so-called artificial neural networks (ANNs), including their RNN variants. Recurrent neural networks utilizing more complex LSTM or GRU units have demonstrated astounding successes in applications requiring

*Correspondence to boh@zurich.ibm.com

learning from temporal data such as speech recognition and language modelling Graves et al. [2013]; He et al. [2019]; Sak et al. [2014]; Sundermeyer et al. [2012]; Fortunato et al. [2019]. Recent works have transferred the rich dynamics of the biologically-inspired SNNs to RNNs and demonstrated on-par performance in certain applications by utilizing gradient-based deep learning methods for training Woźniak et al. [2018]; Bellec et al. [2020]. Typically, the aforementioned models are trained with the ubiquitous BPTT algorithm Werbos [1990]. Despite the great successes of BPTT-trained networks, this algorithm has severe limitations in more biologically-realistic scenarios involving online learning from a continuous stream of inputs. This is because BPTT has to track all past activities by unrolling the network in time, which becomes very deep as the input-sequence length increases. For example, a two-second-long spoken input sequence with 1 ms time steps results in a 2000-layer-deep unrolled network.

Truncated BPTT (TBPTT) reduces the amount of information that needs to be stored by splitting the input stream into shorter segments and updating the parameters of the network after each segment Williams and Zipser [1995]. However, it still leads to system-locking problems, due to network unrolling, as well as learning deficiencies in tasks where there are long time lags between the network activity and the feedback from the environment.

Alternatively, online learning algorithms were developed to update the network parameters in real time as the input data arrives. In this manner, they are conceptually similar to the way the biological brain adapts to changing environment conditions. Two such online algorithms were initially introduced in Williams and Zipser [1989]. The first one, real-time recurrent learning (RTRL), applies updates to the parameters at each time step, hence sacrificing gradient-equivalence to BPTT, whereas the second one, which we refer to as RTRL with deferred updates, applies BPTT-equivalent updates at the end of the input sequence. However, both versions of RTRL have higher complexity than BPTT and for this reason remained rarely used in practice.

Recently, online learning algorithms regained popularity and were investigated following two distinct research directions. The first direction focuses on RTRL approximations with reduced computational complexity. It led to the development of various algorithms, for example Unbiased Online Recurrent Optimization (UORO) Tallec and Ollivier [2018], Kronecker Factored RTRL (KF-RTRL) Mujika et al. [2018] or Optimal Kronecker-Sum Approximation of RTRL (OK-RTRL) Benzing et al. [2019], which all provide approximate gradients. The second direction takes inspiration from biological learning systems and is centered around the debate whether and how they employ error backpropagation Lillicrap and Santoro [2019]. Specifically, learning algorithms such as SuperSpike Zenke and Ganguli [2018], Random Feedback Local Online (RFLO) Murray [2019] and E-prop Bellec et al. [2020] were proposed to approximate the gradients under biological constraints, see Marschall et al. [2019] for a summary. Note that these approaches were primarily derived for a single large layer of recurrent units.

In this work, we revisit the formulation of BPTT and propose a novel online learning methodology that clearly separates the gradient computation into two components: spatial and temporal. Because this gradient separation plays a key role, we refer to our algorithm as Online Spatio-Temporal Learning (OSTL). We apply OSTL to SNNs and demonstrate for the first time that SNNs can be trained online with BPTT-equivalent gradients. We show that the common feed-forward deep SNN architectures enable online learning with low computational complexity and comparable performance to BPTT. Moreover, we extend OSTL for training generic RNNs, such as LSTMs, with a special focus on multi-layered networks. Our work complements the approximate RTRL-based approaches and the biologically-plausible learning methods by proposing a unified approach that follows the BPTT-based derivations. The key contributions of this paper are:

- a novel online learning algorithm for training k -layer feed-forward SNNs with clear separation of spatial and temporal gradients and a time complexity of $O(kn^2)$,
- a novel online learning algorithm for shallow feed-forward SNNs with a clear separation of temporal and spatial gradients and a time complexity of $O(n^2)$, while maintaining the gradient equivalence with BPTT,
- a generalization of this learning algorithm to generic k -layer RNNs with a clear separation of temporal and spatial gradients and a time complexity of $O(kn^4)$,
- an explicit derivation and application of this algorithm to deep recurrent networks comprising spiking neurons, LSTMs or GRUs.

Using this notation, we compute the update of the parameters θ_l that minimizes E based on the principle of gradient descent as

$$\Delta\theta_l = -\eta \frac{dE}{d\theta_l}. \quad (3)$$

From this, we use BPTT as our starting point for the derivation and express $\frac{dE}{d\theta_l}$ as

$$\frac{dE}{d\theta_l} = \sum_{1 \leq t \leq T} \frac{\partial E^t}{\partial y_k^t} \left[\frac{\partial y_k^t}{\partial s_k^t} \frac{ds_k^t}{d\theta_l} + \frac{\partial y_k^t}{\partial \theta_l} \right], \quad (4)$$

where the summation over time ranges from the first time step $t = 1$ until the last time step $t = T$. We further expand Equation 19 below and unravel a recursion that can be exploited to form an online reformulation of BPTT. For the sake of brevity, we outline only the main steps for a single unit, but the detailed derivation is given in Supplementary material S1. In particular, it can be shown that

$$\frac{ds_l^t}{d\theta_l} = \sum_{1 \leq \hat{t} \leq t} \left(\prod_{t \geq t' > \hat{t}} \frac{ds_{l'}^{t'}}{ds_{l'}^{t'-1}} \right) \left(\frac{\partial s_l^{\hat{t}}}{\partial \theta_l} + \frac{\partial s_l^{\hat{t}}}{\partial y_l^{t-1}} \frac{\partial y_l^{t-1}}{\partial \theta_l} \right). \quad (5)$$

Equation 21 can be rewritten in a recursive form as follows

$$\epsilon_l^{t,\theta} := \frac{ds_l^t}{d\theta_l} = \left(\frac{ds_l^t}{ds_l^{t-1}} \epsilon_l^{t-1,\theta} + \left(\frac{\partial s_l^t}{\partial \theta_l} + \frac{\partial s_l^t}{\partial y_l^{t-1}} \frac{\partial y_l^{t-1}}{\partial \theta_l} \right) \right). \quad (6)$$

This leads to an expression of the gradient as

$$\frac{dE}{d\theta_l} = \sum_t L_l^t e_l^{t,\theta} + R, \quad (7)$$

where

$$e_l^{t,\theta} = \left(\frac{\partial y_l^t}{\partial s_l^t} \epsilon_l^{t,\theta} + \frac{\partial y_l^t}{\partial \theta_l} \right) \quad (8)$$

$$L_l^t = \frac{\partial E^t}{\partial y_k^t} \left(\prod_{(k-l+1) \geq m' \geq 1} \frac{\partial y_{k-m'+1}^t}{\partial s_{k-m'+1}^t} \frac{\partial s_{k-m'+1}^t}{\partial y_{k-m'}^t} \right). \quad (9)$$

In order to avoid a cluttered notation we used $\epsilon_l^{t,\theta_l} = \epsilon_l^{t,\theta}$ and $e_l^{t,\theta_l} = e_l^{t,\theta}$. The quantity $e_l^{t,\theta}$ represents the temporal gradients, whereas the quantity L_l^t represents the spatial gradients. Therefore, the parameter update $\frac{dE}{d\theta_l}$ stated in Equation 7 can in principle be calculated as the sum of products of the temporal gradients and the spatial gradients. The residual term R represents combinations of spatial gradients with temporal gradients. Specifically, the term R appears because the total derivative term $\frac{ds_l^t}{d\theta_m}$ in Equation 21 may involve different layers l and m , and thereby introduces dependencies across layers, see Supplementary material S1.

The main goal of OSTL is to maintain the separation between spatial and temporal gradients and therefore, for deep networks, we simplify Equation 7 by omitting the term R . Thus, we obtain the following formulation of OSTL for multi-layer SNNs

$$\frac{dE}{d\theta_l} = \sum_t L_l^t e_l^{t,\theta}. \quad (10)$$

Simulation results in Section 4 indicate that by omitting the residual term R , the approximate OSTL algorithm can achieve very competitive performance to BPTT.

OSTL and in particular the separation of the gradient components are inspired by biological systems, where the change of synaptic weights is often decomposed into a learning signal and an eligibility trace, as for example in the three-factor rules discussed in Gerstner et al. [2018]. The learning signal transports the feedback from the environment to the individual neurons and the eligibility trace is a local signal that provides means for temporal credit assignment. In the simplest case, eligibility traces are low-pass filtered versions of the neural activities, while learning signals represent spatially

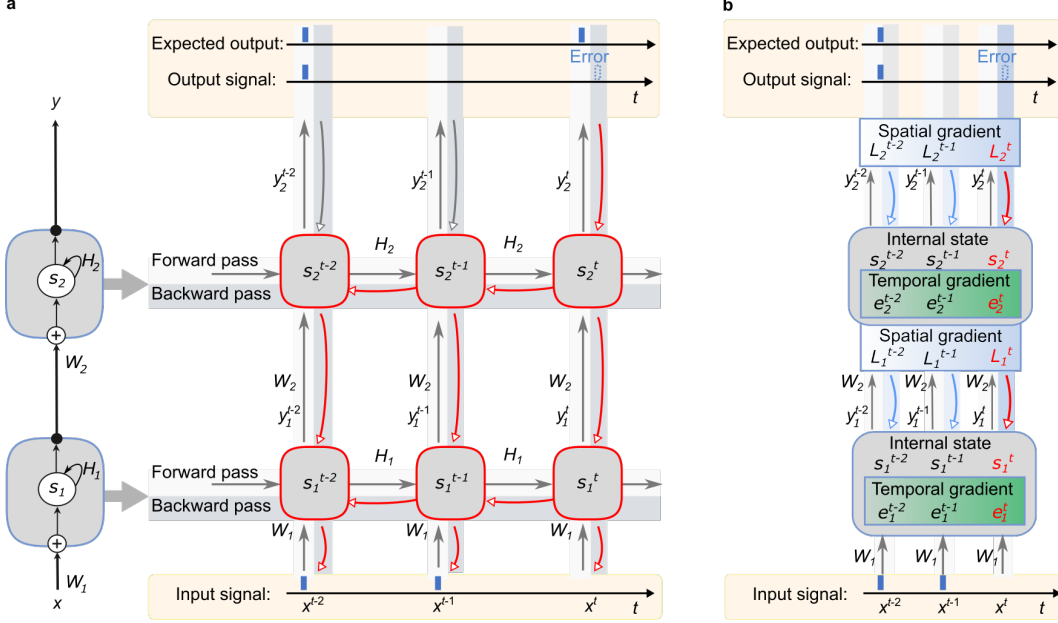


Figure 2: **Gradient flow in a multi-layer RNN over three time steps.** **a**, In BPTT, the unfolded network components involved in the gradient computation at time step t are marked in red. **b**, In OSTL, the spatial and temporal components are clearly separated. Each layer computes eligibility traces which account for the temporal gradients. Independently, an individual learning signal per layer passes from the output layer through the network and accounts for the spatial components. The components involved in the gradient computation at time t are marked in red.

delivered reward signals. Therefore, we naturally associate the temporal gradients denoted as $e_i^{t,\theta}$ in Equation 40 with the eligibility traces and the spatial gradients denoted as L_i^t in Equation 39 with learning signals. Thus, similarly to the three-factor learning rule, $\frac{dE}{d\theta_i}$ stated in Equation 7 is in principle calculated as the sum of products of the eligibility trace and the learning signal. This enables the parameter updates to be computed online, as shown in Figure 2b.

In case of a single recurrent layer, e.g. a large pool of recurrently connected spiking neurons, there is no residual term R emerging in Equation 7, that is $R = 0$. Therefore, OSTL enables the separation of spatial and temporal gradients while maintaining the gradient-equivalence to BPTT, see Supplementary material S2. Moreover, this recurrent layer can be included in a deep network comprising an arbitrary number of stateless layers, e.g. a softmax output layer, without affecting the gradient-equivalence. This important property has also been demonstrated via simulations in Section 4. Supplementary material S3 contains an explicit formulation of OSTL for such network architectures. Note that while the generic form of Equation 10 appears to be similar to works in the literature, for example Bellec et al. [2020], the derivations in Equations 40-39 target deep SNN networks comprising SNUs where not every layer has direct connections to the output. Moreover, we have shown that for shallow networks, even when the spiking neurons are recurrently connected among each other through a matrix H , OSTL provides exact gradients, while the related works rely on approximations.

In the example of a multi-layered feed-forward SNU network outlined above, the explicit form of these equations is

$$e_i^{t,W} = h_l^t \epsilon_l^{t,W} \quad (11)$$

$$e_i^{t,b} = h_l^t \epsilon_l^{t,b} + h_l^t, \quad (12)$$

where

$$\begin{aligned}\epsilon_i^{t,W} &= g_l^t \cdot \left[\frac{ds_l^t}{ds_l^{t-1}} \epsilon_i^{t-1,W} + y_{i-1}^t \right] \\ \epsilon_i^{t,b} &= g_l^t \cdot \left[\frac{ds_l^t}{ds_l^{t-1}} \epsilon_i^{t-1,b} - l(\tau) s_l^{t-1} h_l'^{t-1} \right]\end{aligned}$$

and

$$\frac{ds_l^t}{ds_l^{t-1}} = l(\tau) \left(1 - y_l^{t-1} - s_l^{t-1} h_l'^{t-1} \right). \quad (13)$$

Note that we have used the short-hand notation of $\frac{dg(x_l^t)}{dx_l^t} = g_l^t$ and $\frac{dh(x_l^t)}{dx_l^t} = h_l'^t$. For a mean squared error loss function, i.e., $E^t = (\hat{y}^t - y_k^t)^2$, where \hat{y}^t is the target output, the learning signal is

$$L_l^t = -2(\hat{y}^t - y_k^t) \left(\prod_{(k-l+1) \geq m' \geq 1} h'_{k-m'+1} g'_{k-m'+1} W_{k-m'+1} \right). \quad (14)$$

Algorithm 1 in Supplementary material S1 illustrates in a pseudocode the steps necessary to compute these parameter updates.

This feed-forward SNN network architecture with k layers allows to greatly reduce the computational complexity of OSTL to $O(kn^2)$, compared to $O(kn^4)$ for recurrent multi-layered SNNs. In the latter case, the time complexity is primarily dominated by the recurrency matrix H_l , see Supplementary material S4 for detailed information regarding the stored matrices and their sizes for deep feed-forward and recurrent SNNs. Importantly, using a feed-forward SNU-based network architecture does not necessarily prevent solving temporal tasks. Such networks have long been used in SNNs and it implies that the network should rely on the internal states of the units, implemented using self-recurrency, rather than on layer-wise recurrency matrices H_l .

3 Generalization of OSTL to generic recurrent neural networks

In this section, we extend OSTL to generic deep recurrent neural networks, for example consisting of LSTM units. We note that such units obey a more complex state and output equations compared to the formulation used in OSTL for SNNs. In particular, the output y_l^t is a recursive function of itself and in addition depends on the output of the previous layer and the trainable parameters, that is:

$$y_l^t = f(s_l^t, y_l^{t-1}, y_{l-1}^t, \theta_l), \quad (15)$$

$$s_l^t = f(s_l^{t-1}, y_l^{t-1}, y_{l-1}^t, \theta_l). \quad (16)$$

To the best of our knowledge, this generalized form covers all RNN units currently used in literature, including LSTMs. Performing similar steps as in Section 2, we derive the eligibility trace for layer l as

$$e_l^{t,\theta} = \frac{\partial y_l^t}{\partial s_l^t} \epsilon_l^{t,\theta} + \frac{\partial y_l^t}{\partial \theta_l} + \frac{\partial y_l^t}{\partial y_l^{t-1}} e_l^{t-1,\theta}. \quad (17)$$

Note that compared to the case of SNNs, the eligibility trace contains an additional recurrent term, which is the eligibility trace of the previous time step $t-1$, i.e. $e_l^{t-1,\theta}$. In consequence, these formulations expand the form of the eligibility traces of a particular neuron to depend also on non-local activities of other neurons within the same layer. Nevertheless, the core function of the eligibility traces, to capture the temporal gradient contributions, is maintained.

The generalized output definition leads to the following learning signal

$$L_l^t = \frac{\partial E^t}{\partial y_k^t} \left(\prod_{(k-l+1) \geq m' \geq 1} \left[\frac{\partial y_{k-m'+1}^t}{\partial s_{k-m'+1}^t} \frac{\partial s_{k-m'+1}^t}{\partial y_{k-m'}^t} + \frac{\partial y_{k-m'+1}^t}{\partial y_{k-m'}^t} \right] \right). \quad (18)$$

Finally, similarly to the deep SNN case, the parameter update $\frac{dE}{d\theta_l}$ can be computed using Equation 10. The OSTL extension described in Equations 17-18 enables online training for a broad variety of RNN units, including LSTMs and GRUs, while maintaining the clear separation of temporal and spatial gradient components. The explicit formulas can be found in Supplementary material S5 and S6, respectively. The complexity and the BPTT gradient equivalence of all OSTL versions along with a comparison to other algorithms from related works are summarized in Table 1.

Table 1: Complexity comparison for a single parameter update of OSTL and algorithms from literature. The complexities correspond to single-layer neural networks unless otherwise indicated.

ALGORITHM	MEMORY COMPLEXITY	TIME COMPLEXITY	EXACT GRADIENTS (VS. BPTT)
BPTT (UNROLLED FOR T TIME STEPS)	Tn	Tn^2	✓
RTRL WITH DEFERRED UPDATES	n^3	n^4	✓
RTRL	n^3	n^4	×
UORO	n^2	n^2	×
RFKFRL	n^2	n^3	×
OK-RTRL (FOR r SUMMATION TERMS)	rn^2	rn^3	×
DNI	n^2	n^2	×
RFLO	n^2	n^2	×
SUPERSPIKE (FOR INTEGRATION PERIOD T)	n^2	Tn^2	×
E-PROP	n^2	n^2	×
OSTL	n^3	n^4	✓
OSTL (k LAYERS)	kn^3	kn^4	×
OSTL: FEED-FORWARD SNNs	n^2	n^2	✓
OSTL: FEED-FORWARD SNNs (k LAYERS)	kn^2	kn^2	×

4 Results

We evaluated the performance of OSTL on four tasks: music prediction, handwritten digit classification, language modelling and speech recognition. For each task, we compared the accuracy of OSTL with that of BPTT-based training to highlight the various aspects of our approach. The detailed specifics for each task are described in Supplementary material S7.

Firstly, for the music prediction task based on the JSB dataset Boulanger-Lewandowski et al. [2012], we employed an architecture comprising an RNN layer with 150 units and a stateless output layer comprising 88 sigmoid units, as in Woźniak et al. [2018]. In particular, we analyzed three types of RNN layers, an SNU layer, an sSNU layer as well as an LSTM layer. For this architecture, OSTL provides a low-complexity formulation with BPTT-equivalent gradients. In order to demonstrate this aspect, the same networks, including all its hyperparameters, were trained with OSTL and BPTT. As shown in Figure 3a, the results obtained with OSTL are on par with these obtained with BPTT, thereby empirically validating, via simulations, the gradient equivalence of BPTT and OSTL for such architectures.

The second task illustrates the low-complexity formulation of OSTL for deep feed-forward SNNs using the handwritten digit recognition MNIST dataset Lecun et al. [1998]. In particular, we employed two hidden layers of 256 units each followed by 10 output units. Note that all units were of SNU or sSNU type. Following the standard SNN convention, we used biologically-inspired rate coding that introduces a temporal aspect to this dataset by coding the grey scale values of the pixels in the rates of input spikes generated from a Poisson distribution Gerstner et al. [1997]. As discussed in Section 2, it is possible to train online such a network architecture at a reduced time complexity of $O(kn^2)$. Although our formulation for deep networks omits the residual term R , OSTL achieved competitive classification accuracies to the BPTT baseline as illustrated in Figure 3b.

As a third task, we applied OSTL to language modelling based on the Penn Tree Bank (PTB) dataset Marcus et al. [1993]. To that end, we trained for 20 epochs an architecture comprising a fully-connected layer of 10000 units for embedding, three layers of 1300 feed-forward sSNNs and a softmax output layer of 10000 units. Also in this difficult task, OSTL achieved very competitive performance compared to BPTT, see Figure 3c.

Lastly, we considered an application to speech recognition based on the TIMIT dataset Garofolo [1993]. This task requires to capture long temporal dependencies between the inputs and the outputs, which is especially challenging for TBPTT. We analyze by varying the truncation horizon $T = \{10, 30, 50, 90\}$. The performance of TBPTT is compared to OSTL and BPTT with complete unrolling. For this task we employed a network with 39 input neurons, two layers of 200 feed-forward sSNNs or LSTM units and a softmax output layer of 39 units. The results in Figure 3d show the

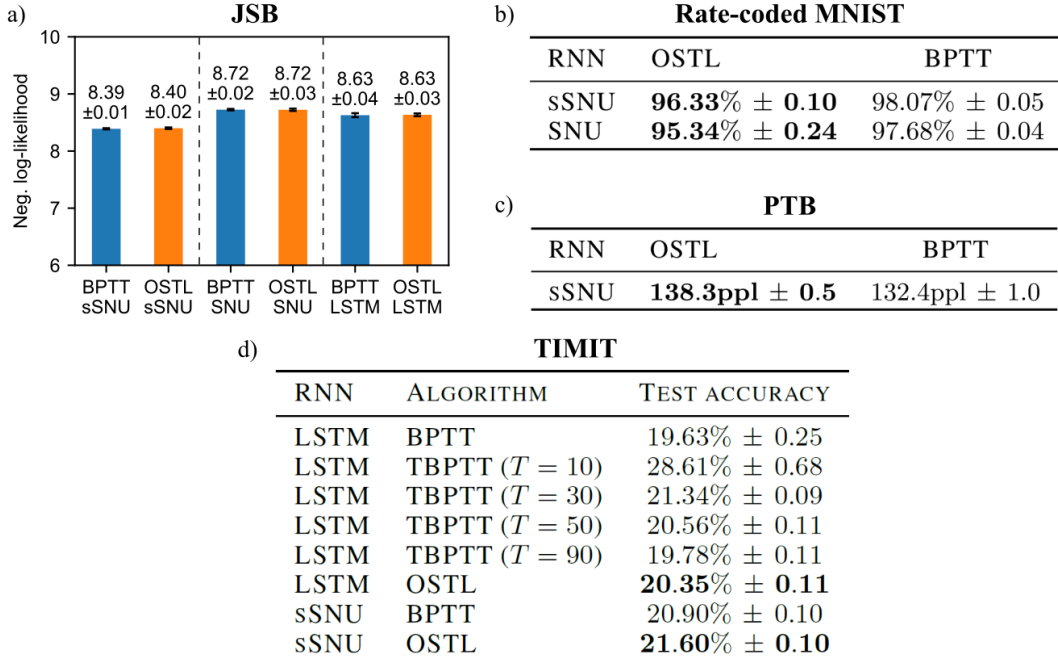


Figure 3: **Test performance** a) JSB dataset trained with BPTT (blue bars) and OSTL (orange bars). The negative log-likelihood loss was used as a performance metric (lower value is better). b) Rate-coded MNIST dataset. We used the classification accuracy for assessment. c) PTB dataset. The perplexity was used as the performance metric (lower value is better). d) TIMIT dataset. T – truncation horizon of TBPTT. For the assesment, the error rate was used (lower value is better).

percentage error rate. The decreasing performance of TBPTT with shorter truncation horizons T indicates that the substantial overhead of unrolling the network far into the past cannot be avoided for this temporal dataset. OSTL in contrast, despite the lack of full BPTT-equivalence for this network architecture, demonstrates competitive performance without unrolling.

5 Conclusion

OSTL is a novel online learning algorithm, whose basic form provides gradients equivalent to those of BPTT and RTRL with deferred updates. However, in contrast to these algorithms, it specifically focuses on the biologically-inspired separation of spatial and temporal gradient components, which facilitates a more efficient development of online learning variants with reduced complexity. In particular, OSTL lends itself to an efficient online training of k -layer feed-forward SNU-based networks with a time complexity of $O(kn^2)$, where the update of the synaptic weights is decomposed into a leaning signal and an eligibility trace as in the three factor rules. Even more so, it enables online training of shallow feed-forward SNNs with BPTT-equivalent gradients and time complexity of $O(n^2)$. Finally, OSTL has been further generalized to deep recurrent network architectures comprising spiking neurons or more complex units, such as LSTMs or GRUs, demonstrating competitive accuracy in comparison to BPTT. The proposed algorithm allows efficient online training for temporal data and opens a new avenue for the adoption of trainable recurrent networks in low-complexity IoT and edge AI devices.

S1 Derivation of OSTL for deep recurrent networks

In this section, we outline the steps in deriving the OSTL algorithm. We start with shallow networks and then expand to deep networks. Specifically, we illustrate the steps for a generic RNN, e.g., a shallow version of the RNN used in Section 2 of the main text. The state and the output equations of such a networks are given by

$$\begin{aligned} s^t &= s^t(x^t, s^{t-1}, y^{t-1}, \theta) \\ y^t &= y^t(s^t, \theta). \end{aligned}$$

The starting point for the derivation is the calculation of the derivative of the loss function E with respect to the parameters θ . Based on the BPTT formulation, we can express $\frac{dE}{d\theta}$ as

$$\frac{dE}{d\theta} = \sum_{1 \leq t \leq T} \frac{\partial E^t}{\partial y^t} \left[\frac{\partial y^t}{\partial s^t} \frac{ds^t}{d\theta} + \frac{\partial y^t}{\partial \theta} \right]. \quad (19)$$

It is shown in Supplementary material S2 that

$$\frac{ds^t}{d\theta} = \sum_{1 \leq \hat{t} \leq t} \left(\prod_{t \geq t' > \hat{t}} \frac{ds^{t'}}{ds^{t'-1}} \right) \left(\frac{\partial s^{\hat{t}}}{\partial \theta} + \frac{\partial s^{\hat{t}}}{\partial y^{\hat{t}-1}} \frac{\partial y^{\hat{t}-1}}{\partial \theta} \right). \quad (20)$$

Therefore, we can expand Equation 19 to

$$\frac{dE}{d\theta} = \sum_{1 \leq t \leq T} \frac{\partial E^t}{\partial y^t} \left[\frac{\partial y^t}{\partial s^t} \sum_{1 \leq \hat{t} \leq t} \left(\prod_{t \geq t' > \hat{t}} \frac{ds^{t'}}{ds^{t'-1}} \right) \left(\frac{\partial s^{\hat{t}}}{\partial \theta} + \frac{\partial s^{\hat{t}}}{\partial y^{\hat{t}-1}} \frac{\partial y^{\hat{t}-1}}{\partial \theta} \right) + \frac{\partial y^t}{\partial \theta} \right]. \quad (21)$$

We analyze the term $\frac{ds^t}{d\theta}$ from Equation 20. At time $t + 1$, the term $\frac{ds^{t+1}}{d\theta}$ can be obtained by multiplying all the terms until time t by $\frac{ds^{t+1}}{ds^t}$ and adding the term $\left(\frac{\partial s^{t+1}}{\partial \theta} + \frac{\partial s^{t+1}}{\partial y^t} \frac{\partial y^t}{\partial \theta} \right)$. This leads to the following recursive reformulation of Equation 20

$$\frac{ds^t}{d\theta} = \left(\frac{ds^t}{ds^{t-1}} \frac{ds^{t-1}}{d\theta} + \left(\frac{\partial s^t}{\partial \theta} + \frac{\partial s^t}{\partial y^{t-1}} \frac{\partial y^{t-1}}{\partial \theta} \right) \right). \quad (22)$$

We define the eligibility vector $\epsilon^{t,\theta}$ to be

$$\epsilon^{t,\theta} := \frac{ds^t}{d\theta}, \quad (23)$$

which can also be recursively expressed as,

$$\epsilon^{t,\theta} = \left(\frac{ds^t}{ds^{t-1}} \epsilon^{t-1,\theta} + \left(\frac{\partial s^t}{\partial \theta} + \frac{\partial s^t}{\partial y^{t-1}} \frac{\partial y^{t-1}}{\partial \theta} \right) \right). \quad (24)$$

Note that this equation corresponds to Equation 6 of the main text. For the first time step $t = 1$, the eligibility vector has the special form

$$\epsilon^{1,\theta} = \frac{ds^1}{d\theta} = \frac{\partial s^1}{\partial \theta}. \quad (25)$$

Next, we rewrite Equation 21 using Equation 24 to

$$\begin{aligned} \frac{dE}{d\theta} &= \sum_{1 \leq t \leq T} \frac{\partial E^t}{\partial y^t} \left[\frac{\partial y^t}{\partial s^t} \left(\frac{ds^t}{ds^{t-1}} \epsilon^{t-1,\theta} + \left(\frac{\partial s^t}{\partial \theta} + \frac{\partial s^t}{\partial y^{t-1}} \frac{\partial y^{t-1}}{\partial \theta} \right) \right) + \frac{\partial y^t}{\partial \theta} \right] \\ &= \sum_{1 \leq t \leq T} L^t \left[\frac{\partial y^t}{\partial s^t} \left(\frac{ds^t}{ds^{t-1}} \epsilon^{t-1,\theta} + \left(\frac{\partial s^t}{\partial \theta} + \frac{\partial s^t}{\partial y^{t-1}} \frac{\partial y^{t-1}}{\partial \theta} \right) \right) + \frac{\partial y^t}{\partial \theta} \right] \\ &= \sum_{1 \leq t \leq T} L^t \left[\frac{\partial y^t}{\partial s^t} \epsilon^{t,\theta} + \frac{\partial y^t}{\partial \theta} \right] \\ &= \sum_{1 \leq t \leq T} L^t e^{t,\theta}, \end{aligned} \quad (26)$$

where we define the eligibility trace $e^{t,\theta}$ and the learning signal L^t as

$$e^{t,\theta} := \frac{dy^t}{d\theta} = \frac{\partial y^t}{\partial s^t} \epsilon^{t,\theta} + \frac{\partial y^t}{\partial \theta} \quad (27)$$

$$L^t := \frac{\partial E^t}{\partial y^t}. \quad (28)$$

Thus we have shown that $\frac{dE}{d\theta}$ can be calculated as the sum of a learning signal, Equation 28, and an eligibility trace, Equation 27.

As outlined in the main text, many state-of-the-art applications rely on multi-layer networks. In such architectures, the error E^t is only a function of the last output layer k , i.e., $E^t = E^t(y_k^t)$. To extend OSTL to these architectures, the state and output equations are adapted as follows

$$s_l^t = s_l^t(s_l^{t-1}, y_l^{t-1}, y_{l-1}^t, \theta_l) \quad (29)$$

$$y_l^t = y_l^t(s_l^t, \theta_l). \quad (30)$$

Using this reformulation, Equation 19 can be generalized as follows

$$\frac{dE}{d\theta_l} = \sum_{1 \leq t \leq T} \frac{dE^t}{d\theta_l} = \sum_{1 \leq t \leq T} \frac{\partial E^t}{\partial y_k^t} \left[\frac{\partial y_k^t}{\partial s_k^t} \frac{ds_k^t}{d\theta_l} + \frac{\partial y_k^t}{\partial \theta_l} \right]. \quad (31)$$

For the last layer of a multi-layer network, where $k = l$, Equation 31 corresponds to Equation 19 for a single layer. However, for the hidden layers, i.e., $k \neq l$, the term $\frac{ds_k^t}{d\theta_l}$ is expanded as follows

$$\frac{ds_k^t}{d\theta_l} = \frac{\partial s_k^t}{\partial \theta_l} + \frac{\partial s_k^t}{\partial y_k^{t-1}} \frac{dy_k^{t-1}}{d\theta_l} + \frac{\partial s_k^t}{\partial y_{k-1}^t} \frac{dy_{k-1}^t}{d\theta_l}. \quad (32)$$

We define a recursive term $\chi_m^{t,\theta}$ as

$$\begin{aligned} \chi_m^{t,\theta} &:= \frac{ds_l^t}{d\theta_m} \\ &= \frac{\partial s_l^t}{\partial s_m^{t-1}} \chi_m^{t-1,\theta} + \frac{\partial s_l^t}{\partial y_l^{t-1}} \left(\frac{\partial y_l^{t-1}}{\partial s_l^{t-1}} \chi_m^{t-1,\theta} + \frac{\partial y_l^{t-1}}{\partial \theta_m} \right) \\ &\quad + \frac{\partial s_l^t}{\partial y_{l-1}^t} \left(\frac{\partial y_{l-1}^t}{\partial s_{l-1}^t} \chi_{l-1}^{t,\theta} + \frac{\partial y_{l-1}^t}{\partial \theta_m} \right) + \frac{\partial s_l^t}{\partial \theta_m}, \end{aligned} \quad (33)$$

with the following properties

$$\epsilon_l^{t,\theta} := \chi_l^{t,\theta} \quad (34)$$

$$e_l^{t,\theta} := \frac{dy_l^t}{d\theta_l} = \left(\frac{\partial y_l^t}{\partial s_l^t} \chi_l^{t,\theta} + \frac{\partial y_l^t}{\partial \theta_l} \right) \quad (35)$$

$$\chi_m^{t < 1, \theta} = 0$$

$$\chi_{l+1}^{t,\theta} = 0$$

$$\chi_{l < 1}^{t,\theta} = 0$$

$$\chi_{m < 1}^{t,\theta} = 0.$$

The term $\chi_m^{t,\theta}$ for $k \neq l$ contains a recursion in time, similar to Equation 22, but additionally it contains a recursion in space, i.e., it depends on other layers, for example the $(k-1)$ -th layer (see Equation 20).

If we insert the term $\chi_m^{t,\theta}$ in Equation 31 we obtain

$$\frac{dE}{d\theta_l} = \sum_{1 \leq t \leq T} \frac{\partial E^t}{\partial y_k^t} \left[\frac{\partial y_k^t}{\partial s_k^t} \chi_k^{t,\theta} + \frac{\partial y_k^t}{\partial \theta_l} \right]. \quad (36)$$

The right-hand side of Equation 36 is expanded to a more complex expression

$$\begin{aligned} \frac{dE}{d\theta_l} = & \sum_{1 \leq t \leq T} \left[\frac{dE^t}{dy_k^t} \left[\frac{\partial y_k^t}{\partial s_k^t} \frac{\partial s_k^t}{\partial s_k^{t-1}} \chi_l^{t-1, \theta} + \frac{\partial y_k^t}{\partial s_k^t} \frac{\partial s_k^t}{\partial y_k^{t-1}} \left(\frac{\partial y_k^{t-1}}{\partial s_k^{t-1}} \chi_l^{t-1, \theta} + \frac{\partial y_k^{t-1}}{\partial \theta_l} \right) \right] \right. \\ & + \frac{\partial y_k^t}{\partial s_k^t} \frac{\partial s_k^t}{\partial y_{k-1}^t} \left(\frac{\partial y_{k-1}^t}{\partial s_{k-1}^t} \chi_{k-1}^{t, \theta} + \frac{\partial y_{k-1}^t}{\partial \theta_l} \right) + \frac{\partial y_k^t}{\partial s_k^t} \frac{\partial s_k^t}{\partial \theta_l} \left. \right] \\ & + \frac{\partial y_k^t}{\partial \theta_l} \Big], \end{aligned} \quad (37)$$

where the two recurrences — $\chi_{k-1}^{t, \theta}$ in space, and $\chi_k^{t-1, \theta}$ in time — become apparent. When expanding χ_{k-1}^t far enough in space, it eventually reaches $\chi_l^{t, \theta} = \epsilon_l^t$. Therefore, we can rewrite Equation 37 as

$$\frac{dE}{d\theta_l} = \sum_{1 \leq t \leq T} \left[\frac{dE^t}{dy_k^t} \left(\prod_{(k-l+1) \geq m' \geq 1} \frac{\partial y_{k-m'+1}^t}{\partial s_{k-m'+1}^t} \frac{\partial s_{k-m'+1}^t}{\partial y_{k-m'}^t} \right) \left(\frac{\partial y_l^t}{\partial s_l^t} \chi_l^{t, \theta} + \frac{\partial y_l^t}{\partial \theta_l} \right) + R \right], \quad (38)$$

where we collect all the remaining terms into a residual term R . In addition, we define a generalized learning signal L_l^t and a generalized eligibility trace $e_l^{t, \theta}$ as

$$L_l^t = \frac{\partial E^t}{\partial y_k^t} \left(\prod_{(k-l+1) \geq m' \geq 1} \frac{\partial y_{k-m'+1}^t}{\partial s_{k-m'+1}^t} \frac{\partial s_{k-m'+1}^t}{\partial y_{k-m'}^t} \right) \quad (39)$$

$$e_l^{t, \theta} = \left(\frac{\partial y_l^t}{\partial s_l^t} \epsilon_l^{t, \theta} + \frac{\partial y_l^t}{\partial \theta_l} \right), \quad (40)$$

see Equations 8-9 of the main text. This allows to express the parameter update as

$$\frac{dE}{d\theta_l} = \sum_{1 \leq t \leq T} \left[L_l^t e_l^{t, \theta} + R \right], \quad (41)$$

see Equation 7 of the main text. By omitting the residual term R , we arrive at the simplified approximate expression of OSTL for deep recurrent networks.

Algorithm 1 summarizes the steps necessary to compute the online parameter updates of OSTL in the form of a pseudocode.

S2 Proof of the equivalence of OSTL and BPTT

In this section, we show the equivalence between BPTT and OSTL for a single layer of recurrently connected units. To that end, we need to establish the following equality

$$\frac{ds^t}{d\theta} \stackrel{!}{=} \sum_{1 \leq \hat{t} \leq t} \left(\prod_{t \geq t' > \hat{t}} \frac{ds^{t'}}{ds^{t'-1}} \right) \left(\frac{\partial s^{\hat{t}}}{\partial \theta} + \frac{\partial s^{\hat{t}}}{\partial y^{\hat{t}-1}} \frac{\partial y^{\hat{t}-1}}{\partial \theta} \right). \quad (42)$$

More specifically, this implies that the term $\frac{ds^t}{d\theta}$, using the chain rule in BPTT, can be also written as a sum of products of derivatives

$$\frac{\partial s^t}{\partial \theta} + \frac{\partial s^t}{\partial s^{t-1}} \frac{ds^{t-1}}{d\theta} + \frac{\partial s^t}{\partial y^{t-1}} \frac{dy^{t-1}}{d\theta} \dots \stackrel{!}{=} \sum_{1 \leq \hat{t} \leq t} \left(\prod_{t \geq t' > \hat{t}} \frac{ds^{t'}}{ds^{t'-1}} \right) \left(\frac{\partial s^{\hat{t}}}{\partial \theta} + \frac{\partial s^{\hat{t}}}{\partial y^{\hat{t}-1}} \frac{\partial y^{\hat{t}-1}}{\partial \theta} \right). \quad (43)$$

To establish the equality of Equation 42 we resort to a proof by induction. The induction basis for the first step of $t = 1$ becomes

$$\left. \frac{ds^t}{d\theta} \right|_{t=1} = \frac{ds^1}{d\theta} = \frac{\partial s^1}{\partial \theta} \quad (44)$$

Algorithm 1 OSTL for deep networks

Input: Parameters $(\theta_l)_{l=1,\dots,k}$, Training data (x_0^t, \hat{y}_k^t) , $t = 1, \dots, T$, Learning rate η

Output: Parameter update $(\Delta\theta_l)_{l=1,\dots,k}$

Initialization (e.g.,: $(s_l^0 = y_l^0 = \epsilon_l^{0,\theta} = \Delta\theta_l = 0)_{l=1,\dots,k}$ and $y_0^1 = x_0^1$)

for $1 \leq t \leq T$ **do**

for $1 \leq l \leq k$ **do**

 Compute s_l^t with $y_{l-1}^t, s_l^{t-1}, y_l^{t-1}, \theta_l$

 Compute y_l^t with s_l^t, θ_l

$$\epsilon_l^{t,\theta} = \left(\frac{ds_l^t}{ds_l^{t-1}} \epsilon_l^{t-1,\theta} + \left(\frac{\partial s_l^t}{\partial \theta_l} + \frac{\partial s_l^t}{\partial y_{l-1}^{t-1}} \frac{\partial y_{l-1}^{t-1}}{\partial \theta_l} \right) \right)$$

$$e_l^{t,\theta} = \frac{\partial y_l^t}{\partial s_l^t} \epsilon_l^{t,\theta} + \frac{\partial y_l^t}{\partial \theta_l}$$

end for

 Compute E^t with y_k^t, \hat{y}^t

for $1 \leq l \leq k$ **do**

$$L_l^t = \frac{\partial E^t}{\partial y_k^t} \left(\prod_{(k-l+1) \geq m' \geq 1} \frac{\partial y_{k-m'+1}^t}{\partial s_{k-m'+1}^t} \frac{\partial s_{k-m'+1}^t}{\partial y_{k-m'}^t} \right)$$

$$\Delta\theta_l = \Delta\theta_l - \eta \left(L_l^t e_l^{t,\theta} \right)$$

end for

end for

for the left-hand side and

$$\sum_{1 \leq \hat{t} \leq t} \left(\prod_{t \geq t' > \hat{t}} \frac{ds^{t'}}{ds^{t'-1}} \right) \left(\frac{\partial s^{\hat{t}}}{\partial \theta} + \frac{\partial s^{\hat{t}}}{\partial y^{\hat{t}-1}} \frac{\partial y^{\hat{t}-1}}{\partial \theta} \right) \Bigg|_{t=1} = \sum_{1 \leq \hat{t} \leq 1} \left(\frac{\partial s^{\hat{t}}}{\partial \theta} + \frac{\partial s^{\hat{t}}}{\partial y^{\hat{t}-1}} \frac{\partial y^{\hat{t}-1}}{\partial \theta} \right) = \frac{\partial s^1}{\partial \theta} \quad (45)$$

for the right-hand side.

Having verified the induction basis, the induction step needs to be investigated next.

$$\frac{ds^{n+1}}{d\theta} = \frac{ds^{n+1}}{ds^n} \frac{ds^n}{d\theta} + \frac{\partial s^{n+1}}{\partial y^n} \frac{\partial y^n}{\partial \theta} + \frac{\partial s^{n+1}}{\partial \theta} \quad (46)$$

$$= \left(\frac{ds^{n+1}}{ds^n} \right) \left[\sum_{1 \leq \hat{t} \leq n} \left(\prod_{n \geq t' > \hat{t}} \frac{ds^{t'}}{ds^{t'-1}} \right) \left(\frac{\partial s^{\hat{t}}}{\partial \theta} + \frac{\partial s^{\hat{t}}}{\partial y^{\hat{t}-1}} \frac{\partial y^{\hat{t}-1}}{\partial \theta} \right) \right] + \frac{\partial s^{n+1}}{\partial y^n} \frac{\partial y^n}{\partial \theta} + \frac{\partial s^{n+1}}{\partial \theta}$$

$$= \left[\sum_{1 \leq \hat{t} \leq n} \left(\prod_{n+1 \geq t' > \hat{t}} \frac{ds^{t'}}{ds^{t'-1}} \right) \left(\frac{\partial s^{\hat{t}}}{\partial \theta} + \frac{\partial s^{\hat{t}}}{\partial y^{\hat{t}-1}} \frac{\partial y^{\hat{t}-1}}{\partial \theta} \right) \right] + \frac{\partial s^{n+1}}{\partial y^n} \frac{\partial y^n}{\partial \theta} + \frac{\partial s^{n+1}}{\partial \theta}$$

$$\frac{ds^{n+1}}{d\theta} = \sum_{1 \leq \hat{t} \leq n+1} \left(\prod_{n+1 \geq t' > \hat{t}} \frac{ds^{t'}}{ds^{t'-1}} \right) \left(\frac{\partial s^{\hat{t}}}{\partial \theta} + \frac{\partial s^{\hat{t}}}{\partial y^{\hat{t}-1}} \frac{\partial y^{\hat{t}-1}}{\partial \theta} \right). \quad (47)$$

By comparing Equation 47 with the hypothesis in Equation 42 for $t = n + 1$, it is evident that this induction step is also fulfilled, which completes the proof.

S3 OSTL applied to recurrent layers embedded in stateless networks

In many network architectures, a recurrent layer is embedded in an arbitrary number of non-recurrent, stateless layers, for example a recurrent layer with a softmax output layer. From the perspective of OSTL, a stateless layer does not introduce any residual term R and therefore OSTL maintains gradient equivalence with BPTT even for deep architectures. To demonstrate this, we consider a deep network consisting of stateless layers, with the following state and output equations

$$s_l^t = s_l^t(y_{l-1}^t, \theta_l) \quad (48)$$

$$y_l^t = y_l^t(s_l^t, \theta_l). \quad (49)$$

These equations simplify the term $\chi_m^{t,\theta}$ from Equation 33 to:

$$\chi_m^{t,\theta} = \frac{\partial s_l^t}{\partial y_{l-1}^t} \left(\frac{\partial y_{l-1}^t}{\partial s_{l-1}^t} \chi_{l-1}^{t,\theta} + \frac{\partial y_{l-1}^t}{\partial \theta_m} \right) + \frac{\partial s_l^t}{\partial \theta_m}. \quad (50)$$

If we insert this term to Equation 36, we obtain

$$\frac{dE}{d\theta_l} = \sum_{1 \leq t \leq T} \left[\frac{dE^t}{dy_k^t} \left[\frac{\partial y_k^t}{\partial s_k^t} \frac{\partial s_k^t}{\partial y_{k-1}^t} \left(\frac{\partial y_{k-1}^t}{\partial s_{k-1}^t} \chi_{l-1}^{t,\theta} + \frac{\partial y_{k-1}^t}{\partial \theta_l} \right) + \frac{\partial y_k^t}{\partial s_k^t} \frac{\partial s_k^t}{\partial \theta_l} \right] + \frac{\partial y_k^t}{\partial \theta_l} \right]. \quad (51)$$

When recursively inserting Equation 50 into Equation 51 until $k - m = l$, most terms include partial derivatives of the form $\frac{\partial y_{k-m}^t}{\partial \theta_l}$ or $\frac{\partial s_{k-m}^t}{\partial \theta_l}$. These terms vanish because the layer $k - m$ does not depend on parameters θ_l , except where $k - m = l$. Therefore, Equation 51 can be written as

$$\frac{dE}{d\theta_l} = \sum_{1 \leq t \leq T} \left[\frac{dE^t}{dy_k^t} \left(\prod_{(k-l+1) \geq m' \geq 1} \frac{\partial y_{k-m'+1}^t}{\partial s_{k-m'+1}^t} \frac{\partial s_{k-m'+1}^t}{\partial y_{k-m'}^t} \right) \left(\frac{\partial y_l^t}{\partial s_l^t} \chi_l^{t,\theta} + \frac{\partial y_l^t}{\partial \theta_l} \right) \right], \quad (52)$$

which is the combination of the generalized learning signal L_l^t and eligibility trace $e_l^{t,\theta}$ without any residual term R , as stated in Equations 41

$$\frac{dE}{d\theta_l} = \sum_{1 \leq t \leq T} L_l^t e_l^{t,\theta}. \quad (53)$$

S4 Complexity analysis

In this section we investigate the computational complexity of OSTL for a single RNN layer. The majority of the computations arises from calculating the eligibility vectors as given in Equation 24. Specifically, the term $\frac{ds_i^t}{ds_l^{t-1}} \epsilon^{t-1, \theta}$ is computationally the most intensive one, as it requires matrix multiplications. We use the index notation to explicitly investigate the complexity in terms of the number of multiplications involved

$$\begin{aligned} \epsilon_{ijk}^{t, \theta} &= \left(\frac{ds_i^t}{ds_l^{t-1}} \epsilon_{ijk}^{t-1, \theta} + \left(\frac{\partial s_i^t}{\partial \theta_{jk}} + \frac{\partial s_i^t}{\partial y_l^{t-1}} \frac{\partial y_l^{t-1}}{\partial \theta_{jk}} \right) \right) \\ \epsilon_{ijk}^{t, \theta} &\sim \frac{ds_i^t}{ds_l^{t-1}} \epsilon_{ijk}^{t-1, \theta}. \end{aligned} \quad (54)$$

Thus we observe

$$\begin{aligned} \epsilon_{ijk}^{t, \theta} &\sim O(n) \\ \epsilon^{t, \theta} &\sim O(n^4). \end{aligned} \quad (55)$$

In particular, computing a single value of the eligibility vector $\epsilon_{ijk}^{t, \theta}$ requires $O(n)$ multiplications, where n denotes the number of units in the layer. Therefore, the total computational cost of OSTL for shallow RNNs is $O(n^4)$ as stated in Tab. 1 of the main text. In case of a multi-layered architecture, this complexity is scaled by the number of layers, e.g., $O(kn^4)$, where k denotes the number of layers and $n = \max_{1 \leq l \leq k} n_l$ denotes the maximum number of units in any layer.

However, if we analyze a feed-forward SNN with the state and output equations given by Equations 1-2 of the main text, the eligibility vector $\epsilon_{ijk}^{t, \theta}$ reduces to a rank-two tensor, because the Jacobian $\frac{ds_i^t}{ds_l^{t-1}}$ reduces to a diagonal matrix as

$$\begin{aligned} \epsilon_{ijk}^{t, \theta} &= \left(\frac{ds_i^t}{ds_l^{t-1}} \delta_{il} \epsilon_{ijk}^{t-1, \theta} + \left(\frac{\partial s_i^t}{\partial \theta_{jk}} \delta_{ik} + \frac{\partial s_i^t}{\partial y_l^{t-1}} \delta_{il} \frac{\partial y_l^{t-1}}{\partial \theta_{jk}} \delta_{ik} \right) \right) \\ \epsilon_{ij}^{t, \theta} &\sim \frac{ds_i^t}{ds_l^{t-1}} \delta_{il} \epsilon_{ij}^{t-1, \theta} \\ &\sim \frac{ds_i^t}{ds_l^{t-1}} \epsilon_{ij}^{t-1, \theta}. \end{aligned} \quad (56)$$

Thus we observe that the number of involved multiplications is

$$\epsilon_{ij}^{t, \theta} \sim O(1) \quad (58)$$

$$\epsilon^{t, \theta} \sim O(n^2). \quad (59)$$

This implies that OSTL enables training of shallow feed-forward SNNs with a reduced time complexity of $O(n^2)$ and of $O(kn^2)$ for k -layered feed-forward SNNs.

S5 OSTL for Long Short-Term Memory

Because LSTM units are probably the most commonly used type of RNN unit in contemporary state-of-the-art machine learning applications, we include an explicit derivation of OSTL for LSTM units. An LSTM unit contains three gates and an internal state which are governed by the following state equations

$$i_i^t = g(W^i y_{i-1}^t + H^i y_i^{t-1} + b^i) \quad (60)$$

$$o_i^t = g(W^o y_{i-1}^t + H^o y_i^{t-1} + b^o) \quad (61)$$

$$f_i^t = g(W^f y_{i-1}^t + H^f y_i^{t-1} + b^f) \quad (62)$$

$$s_i^t = f_i^t s_i^{t-1} + i_i^t h(W^s y_{i-1}^t + H^s y_i^{t-1} + b^s) \quad (63)$$

$$\begin{aligned} &= g(W^f y_{i-1}^t + H^f y_i^{t-1} + b^f) s_i^{t-1} + \\ &\quad g(W^i y_{i-1}^t + H^i y_i^{t-1} + b^i) h(W^s y_{i-1}^t + H^s y_i^{t-1} + b^s) \end{aligned} \quad (64)$$

$$y_i^t = o_i^t h(s_i^t) \quad (65)$$

$$= g(W^o y_{i-1}^t + H^o y_i^{t-1} + b^o) h(s_i^t), \quad (66)$$

where typically $g = \sigma$ and $h = \tanh$. Note that we reformulated Equations 64 and 66 such that one can immediately see the resemblance to the generalized Equations 15-16 of the main text.

In order to avoid a cluttered notation, we derive OSTL for a single LSTM unit, by using Equation 40. The eligibility traces take the following form

$$e_i^{t,W^i} = \left(o_i^t h_i^{y,t} \right) \epsilon^{t,W^i} + \left(h_i^{s,t} g_i^{o,t} H^o \right) e_i^{t-1,W^i} \quad (67)$$

$$e_i^{t,H^i} = \left(o_i^t h_i^{y,t} \right) \epsilon^{t,H^i} + \left(h_i^{s,t} g_i^{o,t} H^o \right) e_i^{t-1,H^i} \quad (68)$$

$$e_i^{t,b^i} = \left(o_i^t h_i^{y,t} \right) \epsilon^{t,b^i} + \left(h_i^{s,t} g_i^{o,t} H^o \right) e_i^{t-1,b^i} \quad (69)$$

$$e_i^{t,W^f} = \left(o_i^t h_i^{y,t} \right) \epsilon^{t,W^f} + \left(h_i^{s,t} g_i^{o,t} H^o \right) e_i^{t-1,W^f} \quad (70)$$

$$e_i^{t,H^f} = \left(o_i^t h_i^{y,t} \right) \epsilon^{t,H^f} + \left(h_i^{s,t} g_i^{o,t} H^o \right) e_i^{t-1,H^f} \quad (71)$$

$$e_i^{t,b^f} = \left(o_i^t h_i^{y,t} \right) \epsilon^{t,b^f} + \left(h_i^{s,t} g_i^{o,t} H^o \right) e_i^{t-1,b^f} \quad (72)$$

$$e_i^{t,W^s} = \left(o_i^t h_i^{y,t} \right) \epsilon^{t,W^s} + \left(h_i^{s,t} g_i^{o,t} H^o \right) e_i^{t-1,W^s} \quad (73)$$

$$e_i^{t,H^s} = \left(o_i^t h_i^{y,t} \right) \epsilon^{t,H^s} + \left(h_i^{s,t} g_i^{o,t} H^o \right) e_i^{t-1,H^s} \quad (74)$$

$$e_i^{t,b^s} = \left(o_i^t h_i^{y,t} \right) \epsilon^{t,b^s} + \left(h_i^{s,t} g_i^{o,t} H^o \right) e_i^{t-1,b^s} \quad (75)$$

$$e_i^{t,W^o} = \left(o_i^t h_i^{y,t} \right) \epsilon^{t,W^o} + h_i^{y,t} g_i^{o,t} y_{i-1}^t + \left(h_i^{s,t} g_i^{o,t} H^o \right) e_i^{t-1,W^o} \quad (76)$$

$$e_i^{t,H^o} = \left(o_i^t h_i^{y,t} \right) \epsilon^{t,H^o} + h_i^{y,t} g_i^{o,t} y_{i-1}^t + \left(h_i^{s,t} g_i^{o,t} H^o \right) e_i^{t-1,H^o} \quad (77)$$

$$e_i^{t,b^o} = \left(o_i^t h_i^{y,t} \right) \epsilon^{t,b^o} + h_i^{y,t} g_i^{o,t} + \left(h_i^{s,t} g_i^{o,t} H^o \right) e_i^{t-1,b^o}, \quad (78)$$

using Equation 24 the eligibility vectors in Equations 67-78 become

$$\epsilon_l^{t,W^i} = \frac{ds_l^t}{ds_l^{t-1}} \epsilon_l^{t-1,W^i} + h_l^{s,t} g_l^{i,t} y_{l-1}^t \quad (79)$$

$$\epsilon_l^{t,H^i} = \frac{ds_l^t}{ds_l^{t-1}} \epsilon_l^{t-1,H^i} + h_l^{s,t} g_l^{i,t} y_l^{t-1} \quad (80)$$

$$\epsilon_l^{t,b^i} = \frac{ds_l^t}{ds_l^{t-1}} \epsilon_l^{t-1,b^i} + h_l^{s,t} g_l^{i,t} \quad (81)$$

$$\epsilon_l^{t,W^f} = \frac{ds_l^t}{ds_l^{t-1}} \epsilon_l^{t-1,W^f} + s_l^{t-1} g_l^{f,t} y_{l-1}^t \quad (82)$$

$$\epsilon_l^{t,H^f} = \frac{ds_l^t}{ds_l^{t-1}} \epsilon_l^{t-1,H^f} + s_l^{t-1} g_l^{f,t} y_l^{t-1} \quad (83)$$

$$\epsilon_l^{t,b^f} = \frac{ds_l^t}{ds_l^{t-1}} \epsilon_l^{t-1,b^f} + s_l^{t-1} g_l^{f,t} \quad (84)$$

$$\epsilon_l^{t,W^s} = \frac{ds_l^t}{ds_l^{t-1}} \epsilon_l^{t-1,W^s} + i_l^t h_l^{s,t} y_{l-1}^t \quad (85)$$

$$\epsilon_l^{t,H^s} = \frac{ds_l^t}{ds_l^{t-1}} \epsilon_l^{t-1,H^s} + i_l^t h_l^{s,t} y_l^{t-1} \quad (86)$$

$$\epsilon_l^{t,b^s} = \frac{ds_l^t}{ds_l^{t-1}} \epsilon_l^{t-1,b^s} + i_l^t h_l^{s,t} \quad (87)$$

$$\begin{aligned} \epsilon_l^{t,W^o} &= \frac{ds_l^t}{ds_l^{t-1}} \epsilon_l^{t-1,W^o} + \\ &\quad \left(g_l^{f,t} s_l^{t-1} H^f g_l^{o,t-1} h_l^{y,t-1} y_{l-1}^{t-1} + h_l^{s,t} g_l^{i,t} H^i g_l^{o,t-1} h_l^{y,t-1} y_{l-1}^{t-1} + i_l^t h_l^{s,t} H^s g_l^{o,t-1} h_l^{y,t-1} y_{l-1}^{t-1} \right) \end{aligned} \quad (88)$$

$$\begin{aligned} \epsilon_l^{t,H^o} &= \frac{ds_l^t}{ds_l^{t-1}} \epsilon_l^{t-1,H^o} + \\ &\quad \left(g_l^{f,t} s_l^{t-1} H^f g_l^{o,t-1} h_l^{y,t-1} y_l^{t-2} + h_l^{s,t} g_l^{i,t} H^i g_l^{o,t-1} h_l^{y,t-1} y_l^{t-2} + i_l^t h_l^{s,t} H^s g_l^{o,t-1} h_l^{y,t-1} y_l^{t-2} \right) \end{aligned} \quad (89)$$

$$\begin{aligned} \epsilon_l^{t,b^o} &= \frac{ds_l^t}{ds_l^{t-1}} \epsilon_l^{t-1,b^o} + \\ &\quad \left(g_l^{f,t} s_l^{t-1} H^f g_l^{o,t-1} h_l^{y,t-1} + h_l^{s,t} g_l^{i,t} H^i g_l^{o,t-1} h_l^{y,t-1} + i_l^t h_l^{s,t} H^s g_l^{o,t-1} h_l^{y,t-1} \right), \end{aligned} \quad (90)$$

with

$$\frac{ds_l^t}{ds_l^{t-1}} = \left(f^t + g_l^{f,t} s_l^{t-1} H^f o_l^{t-1} h_l^{y,t-1} + h_l^{s,t} g_l^{i,t} H^i o_l^{t-1} h_l^{y,t-1} + i_l^t h_l^{s,t} H^s o_l^{t-1} h_l^{y,t-1} \right). \quad (91)$$

We have used the short-hand notation of $\frac{d\psi^t}{d\omega^t} = g_l^{\psi,t} = g_l^{\psi,t}$ with $\psi = \{i, o, f, s\}$ and $\omega = \{y_l^{t-1}, \theta_l\}$, $h(s_l^t) = h_l^{y,t}$, $\frac{dh(s_l^t)}{ds_l^t} = h_l^{y,t}$, $h(W^s y_{l-1}^t + H^s y_l^{t-1} + b^s) = h_l^{s,t}$ and $\frac{dh(W^s y_{l-1}^t + H^s y_l^{t-1} + b^s)}{d\omega} = h_l^{\psi,t} |_{W^s y_{l-1}^t + H^s y_l^{t-1} + b^s} = h_l^{\psi,t}$, with $\omega = \{y_l^{t-1}, \theta_l\}$.

S6 OSTL for Gated Recurrent Unit

OSTL can also be applied to GRUs. To illustrate this, we start from the state equations

$$u_l^t = g(W^u y_{l-1}^t + H^u s_l^{t-1} + b^u) \quad (92)$$

$$r_l^t = g(W^r y_{l-1}^t + H^r s_l^{t-1} + b^o) \quad (93)$$

$$\begin{aligned} s_l^t &= u_l^t s_l^{t-1} + (1 - u_l^t) h(W^c y_{l-1}^t + H^c (r_l^t s_l^{t-1}) + b^c) \\ &= g(W^u y_{l-1}^t + H^u s_l^{t-1} + b^u) s_l^{t-1} + \\ &\quad (1 - g(W^u y_{l-1}^t + H^u s_l^{t-1} + b^u)) h(W^c y_{l-1}^t + H^c (g(W^r y_{l-1}^t + H^r s_l^{t-1} + b^o) s_l^{t-1}) + b^c), \end{aligned} \quad (94)$$

where typically $g = \sigma$ and $h = \tanh$. Note that we reformulated Equations 95 such that one can immediately see the resemblance to the generalized Equations 15 of the main text.

As one can see, a GRU does not have a separate output equation. Therefore, in order to remain consistent with the previous notation and to apply OSTL, we introduce a simple output equation

$$y_l^t = s_l^t, \quad (96)$$

which does not change the behavior of the GRU.

Using this formulation, the eligibility traces can be calculated according to Equation 40 as

$$e_l^{t,W^u} = \epsilon_l^{t,W^u} \quad (97)$$

$$e_l^{t,H^u} = \epsilon_l^{t,H^u} \quad (98)$$

$$e_l^{t,b^u} = \epsilon_l^{t,b^u} \quad (99)$$

$$e_l^{t,W^r} = \epsilon_l^{t,W^r} \quad (100)$$

$$e_l^{t,H^r} = \epsilon_l^{t,H^r} \quad (101)$$

$$e_l^{t,b^r} = \epsilon_l^{t,b^r} \quad (102)$$

$$e_l^{t,W^c} = \epsilon_l^{t,W^c} \quad (103)$$

$$e_l^{t,H^c} = \epsilon_l^{t,H^c} \quad (104)$$

$$e_l^{t,b^c} = \epsilon_l^{t,b^c}, \quad (105)$$

using Equation 24 the eligibility vectors in Equations 97-105 become

$$\epsilon_l^{t,W^u} = \frac{ds_l^t}{ds_l^{t-1}} \epsilon_l^{t-1,W^u} + s_l^{t-1} g_l'^{u,t} y_{l-1}^t - h_l^{s,t} g_l'^{u,t} y_{l-1}^t \quad (106)$$

$$\epsilon_l^{t,H^u} = \frac{ds_l^t}{ds_l^{t-1}} \epsilon_l^{t-1,H^u} + s_l^{t-1} g_l'^{u,t} y_{l-1}^t - h_l^{s,t} g_l'^{u,t} y_{l-1}^t \quad (107)$$

$$\epsilon_l^{t,b^u} = \frac{ds_l^t}{ds_l^{t-1}} \epsilon_l^{t-1,b^u} + s_l^{t-1} g_l'^{u,t} - h_l^{s,t} g_l'^{u,t} \quad (108)$$

$$\epsilon_l^{t,W^r} = \frac{ds_l^t}{ds_l^{t-1}} \epsilon_l^{t-1,W^r} + (1 - u_l^t) h_l'^{s,t} H^c s_l^{t-1} g_l'^{r,t} y_{l-1}^t \quad (109)$$

$$\epsilon_l^{t,H^r} = \frac{ds_l^t}{ds_l^{t-1}} \epsilon_l^{t-1,H^r} + (1 - u_l^t) h_l'^{s,t} H^c s_l^{t-1} g_l'^{r,t} y_{l-1}^t \quad (110)$$

$$\epsilon_l^{t,b^r} = \frac{ds_l^t}{ds_l^{t-1}} \epsilon_l^{t-1,b^r} + (1 - u_l^t) h_l'^{s,t} H^c s_l^{t-1} g_l'^{r,t} \quad (111)$$

$$\epsilon_l^{t,W^c} = \frac{ds_l^t}{ds_l^{t-1}} \epsilon_l^{t-1,W^c} + (1 - u_l^t) h_l'^{s,t} y_{l-1}^t \quad (112)$$

$$\epsilon_l^{t,H^c} = \frac{ds_l^t}{ds_l^{t-1}} \epsilon_l^{t-1,H^c} + (1 - u_l^t) h_l'^{s,t} r_l^t s_l^{t-1} \quad (113)$$

$$\epsilon_l^{t,b^c} = \frac{ds_l^t}{ds_l^{t-1}} \epsilon_l^{t-1,b^c} + (1 - u_l^t) h_l'^{s,t}, \quad (114)$$

with

$$\frac{ds_i^t}{ds_i^{t-1}} = \left(u_i^t + s_i^{t-1} g_l^{u,t} H^u - h_i^{s,t} g_l^{u,t} H^u + (1 - u_i^t) h_i^{s,t} H^c r_i^t + (1 - u_i^t) h_i^{s,t} H^c s_i^{t-1} g_l^{r,t} H^r \right) \quad (115)$$

We used the short-hand notation of $\frac{d\psi_l^t}{d\omega^t} = g'_l|_{\psi_l^t} = g_l^{\psi,t}$ with $\psi = \{i, o, f, s\}$ and $\omega = \{y_i^{t-1}, \theta_l\}$, $h(s_i^t) = h_i^{y,t}$, $\frac{dh(s_i^t)}{ds_i^t} = h_l^{y,t}$, $h(W^s y_{i-1}^t + H^s y_i^{t-1} + b^s) = h_i^{s,t}$ and $\frac{dh(W^s y_{i-1}^t + H^s y_i^{t-1} + b^s)}{d\omega} = h'_l|_{W^s y_{i-1}^t + H^s y_i^{t-1} + b^s} = h_l^{y,t}$.

S7 Simulation setup

The simulations were performed on a standard desktop PC with a single NVIDIA RTX2080 GPU, and for hyperparameter exploration on a supercomputer cluster. For the neural network implementation we used the TensorFlow, version 1.10.0, deep learning framework with GPU support enabled. The detailed hyperparameters for our tasks are described in the following subsections.

S7.1 Music prediction

We used the JSB dataset Boulanger-Lewandowski et al. [2012] with the standard training/testing data split, i.e., 229 chorales for training and 77 chorales for testing. We employed an architecture comprising an RNN layer with 150 units and a stateless output layer comprising 88 sigmoid units, as in Woźniak et al. [2018]. In particular, we analyzed three types of RNN layers, an SNU layer configured to $h = \text{Step}$, $g = I$ and $l(\tau) = 0.4$, an sSNU layer configured to $h = \sigma$, $g = \max(0, x) = \text{ReLU}$ and $l(\tau) = 0.8$, as well as an LSTM layer. We used the standard stochastic gradient descent optimizer and trained with BPTT and OSTL for at least 150 epochs, or until the test performance did not improve for more than 15 epochs. The assessment was done based on the common approach to report the negative log-likelihood. For OSTL we investigated learning rates between $10^{-5} - 10^{-2}$. Our final results were obtained using learning rates of 0.0005, 0.0001 and 0.0003 for the SNU, sSNU and LSTM network, respectively. To ensure repeatability of the results, we averaged them over 5 networks trained with different random initial conditions.

S7.2 Digit classification

We used the MNIST dataset Lecun et al. [1998] with the standard training/testing data split, i.e., 60000 examples for training and 10000 examples for testing. The grey values of the pixels were transformed into spike rates using the same procedure as presented in Woźniak et al. [2018] with $N_s = 20$. We employed a deep feed-forward architecture of two layers of sSNUs with 256 units each and an output layer of 10 sSNUs, all configured to $h = \sigma$, $g = \Theta(x)(x + \alpha x) - \alpha|x| = \text{LReLU}$ (leaky ReLU) with $\alpha = 0.01$ and $l(\tau) = 0.9$. In addition, we employed a feed-forward architecture of two layers of SNUs with 256 units each and an output layer of 10 SNUs, all configured to $h = \text{Step}$, $g = \text{LReLU}$ with $\alpha = 0.01$ and $l(\tau) = 0.9$. We used the standard stochastic gradient descent optimizer and trained for 100 epochs with BPTT and OSTL. The assessment was done based on the classification accuracy. For OSTL we investigated learning rates between $10^{-3} - 0.5$. Our final results were obtained using learning rates of 0.15 and 0.2 for the sSNU and the SNU configuration, respectively. To ensure repeatability of the results, we averaged them over 5 networks trained with different random initial conditions.

S7.3 Language modelling

The PTB dataset Marcus et al. [1993] in a word-level version preprocessed by Tomáš Mikolov PTB was used for language modelling. It comprises sequences of words corresponding to English sentences from the Wall Street Journal, restricted to the most frequent 10k tokens and split into training, validation and test sub sequences with around 930k, 74k and 82k tokens, respectively. We employed an architecture comprising an embedding layer with 10000 units, followed by three feed-forward sSNU layers with 1300 units each, configured to $h = \sigma$, $g = I$ and $l(\tau) = 0.4$, and a softmax layer with 10000 units on top. Note that the weights of the softmax output layer were

tied to the input embeddings. We used the standard stochastic gradient descent optimizer with initial learning rates of 1.0 for BPTT and in the range of $10^{-2} - 1.0$, respectively. Our final results for OSTL were obtained with an initial learning rate of 0.08. The initial learning rates were multiplied by a factor of 0.5 at each epoch if the validation perplexity did not improve by more than 10%. We used gradient clipping with a ratio of 3.5. We trained for at least 20 epochs, or until the validation perplexity did not further decrease, and averaged over 5 random initializations.

S7.4 Speech recognition

We considered an application to speech recognition based on the TIMIT dataset Garofolo [1993]. To this end, we used the same data preprocessing as stated in Greff et al. [2016], but instead of 61 output classes we used the reduced set of 39 output classes. We employed an architecture comprising two layers of LSTMs with 200 units each and a stateless softmax layer with 39 units on top. In addition, we also employed an architecture comprising two layers of sSNUs configured to $h = \sigma$, $g = I$ and $l(\tau) = 0.3$ with 200 units each and a stateless softmax layer with 39 units on top. We used the RMSProp optimizer with a decay of 0.95 and an epsilon of 1^{-8} and trained for 24 epochs with BPTT and OSTL. The assessment was done based on the phoneme error rate. For OSTL we investigated learning rates between $10^{-5} - 10^{-2}$. Our final results were obtained using learning rates of 0.00076 for LSTMs and 0.00083 for sSNUs, respectively. To ensure repeatability of the results, we averaged them over 5 networks trained with different random initial conditions.

References

- Bryan Kolb and Ian Whishaw. Brain plasticity and behavior. *Annual Review of Psychology*, 49:43–64, Feb 1998. doi: 10.1146/annurev.psych.49.1.43.
- C. Mead. Neuromorphic electronic systems. *Proceedings of the IEEE*, 78(10):1629–1636, 1990.
- A. Graves, A. Mohamed, and G. Hinton. Speech recognition with deep recurrent neural networks. In *2013 IEEE International Conference on Acoustics, Speech and Signal Processing*, pages 6645–6649, 2013.
- Y. He, T. N. Sainath, R. Prabhavalkar, I. McGraw, R. Alvarez, D. Zhao, D. Rybach, A. Kannan, Y. Wu, R. Pang, Q. Liang, D. Bhatia, Y. Shangguan, B. Li, G. Pundak, K. C. Sim, T. Bagby, S. Chang, K. Rao, and A. Gruenstein. Streaming end-to-end speech recognition for mobile devices. In *IEEE International Conference on Acoustics, Speech and Signal Processing*, pages 6381–6385, 2019.
- H. Sak, Andrew Senior, and F. Beaufays. Long short-term memory recurrent neural network architectures for large scale acoustic modeling. *Proceedings of the Annual Conference of the International Speech Communication Association*, pages 338–342, Jan 2014.
- Martin Sundermeyer, Ralf Schlüter, and Hermann Ney. LSTM Neural Networks for Language Modeling. *Proceedings of the Annual Conference of the International Speech Communication Association*, pages 194–197, Sep 2012.
- Meire Fortunato, Melissa Tan, Ryan Faulkner, Steven Stenberg Hansen, Adrià Puigdomènech Badia, Gavin Buttimore, Charles Deck, Joel Z. Leibo, and Charles Blundell. Generalization of reinforcement learners with working and episodic memory. In *NeurIPS*, 2019.
- Stanisław Woźniak, Angeliki Pantazi, Thomas Bohnstingl, and Evangelos Eleftheriou. Deep learning incorporating biologically-inspired neural dynamics. *arXiv*, Dec 2018. URL <https://arxiv.org/abs/1812.07040>.
- Guillaume Bellec, Franz Scherr, Anand Subramoney, Elias Hajek, Darjan Salaj, Robert Legenstein, and Wolfgang Maass. A solution to the learning dilemma for recurrent networks of spiking neurons. *bioRxiv*, Apr 2020. doi: 10.1101/738385.
- P. J. Werbos. Backpropagation through time: what it does and how to do it. *Proc. IEEE*, 78(10): 1550–1560, Oct 1990. ISSN 1558-2256. doi: 10.1109/5.58337.

- Ronald J. Williams and David Zipser. *Gradient-based learning algorithms for recurrent networks and their computational complexity*. L. Erlbaum Associates Inc., Jan 1995. ISBN 978-0-8058-1259-6. URL <http://dl.acm.org/citation.cfm?id=201784.201801>.
- Ronald J. Williams and David Zipser. A Learning Algorithm for Continually Running Fully Recurrent Neural Networks. *Neural Comput.*, 1(2):270–280, Jun 1989. ISSN 0899-7667. doi: 10.1162/neco.1989.1.2.270.
- Corentin Tallec and Yann Ollivier. Unbiased online recurrent optimization. In *International Conference on Learning Representations*, 2018. URL <https://openreview.net/forum?id=rJQDjk-0b>.
- Asier Mujika, Florian Meier, and Angelika Steger. Approximating real-time recurrent learning with random kronecker factors. In *Proceedings of the 32nd International Conference on Neural Information Processing Systems, NIPS’18*, pages 6594–6603, 2018. URL <http://dl.acm.org/citation.cfm?id=3327757.3327766>.
- Frederik Benzing, Marcelo Matheus Gauy, Asier Mujika, Anders Martinsson, and Angelika Steger. Optimal kronecker-sum approximation of real time recurrent learning. In *ICML*, pages 604–613, 2019. URL <http://proceedings.mlr.press/v97/benzing19a.html>.
- Timothy P. Lillicrap and Adam Santoro. Backpropagation through time and the brain. *Curr. Opin. Neurobiol.*, 55:82–89, Apr 2019. ISSN 0959-4388. doi: 10.1016/j.conb.2019.01.011.
- Friedemann Zenke and Surya Ganguli. SuperSpike: Supervised Learning in Multilayer Spiking Neural Networks. *Neural Comput.*, May 2018. URL https://www.mitpressjournals.org/doi/full/10.1162/neco_a_01086.
- James M Murray. Local online learning in recurrent networks with random feedback. *eLife*, 8:e43299, May 2019. ISSN 2050-084X. doi: 10.7554/eLife.43299. URL <https://doi.org/10.7554/eLife.43299>.
- Owen Marschall, Kyunghyun Cho, and Cristina Savin. A Unified Framework of Online Learning Algorithms for Training Recurrent Neural Networks. *arXiv*, Jul 2019. URL <https://arxiv.org/abs/1907.02649>.
- Wulfram Gerstner, Marco Lehmann, Vasiliki Liakoni, Dane Corneil, and Johanni Brea. Eligibility Traces and Plasticity on Behavioral Time Scales: Experimental Support of NeoHebbian Three-Factor Learning Rules. *Front. Neural Circuits*, 12, Jul 2018. ISSN 1662-5110. doi: 10.3389/fncir.2018.00053.
- Guillaume Bellec, Franz Scherr, Anand Subramoney, Elias Hajek, Darjan Salaj, Robert Legenstein, and Wolfgang Maass. A solution to the learning dilemma for recurrent networks of spiking neurons. *bioRxiv*, 2019. doi: 10.1101/738385. URL <https://www.biorxiv.org/content/early/2019/12/09/738385>.
- Nicolas Boulanger-Lewandowski, Yoshua Bengio, and Pascal Vincent. Modeling temporal dependencies in high-dimensional sequences: Application to polyphonic music generation and transcription. In *Proceedings of the 29th International Conference on Machine Learning, ICML’12*, page 1881–1888, Madison, WI, USA, 2012. Omnipress. ISBN 9781450312851.
- Y. Lecun, L. Bottou, Y. Bengio, and P. Haffner. Gradient-based learning applied to document recognition. *Proc. IEEE*, 86(11):2278–2324, Nov 1998. ISSN 1558-2256. doi: 10.1109/5.726791.
- Wulfram Gerstner, Andreas Kreiter, Henry Markram, and Andreas Herz. Neural codes: Firing rates and beyond. *Proceedings of the National Academy of Sciences*, 94:12740–12741, Nov 1997. doi: 10.1073/pnas.94.24.12740.
- Mitchell Marcus, M Marcinkiewicz, and Beatrice Santorini. Building a large annotated corpus of English: The Penn Treebank. *Computational Linguistics*, 1993.
- John S Garofolo. TIMIT acoustic phonetic continuous speech corpus. *Linguistic Data Consortium*, 1993.

PTB dataset – Pre-processed. www.fit.vutbr.cz/~imikolov/rnnlm/simple-examples.tgz.
Accessed: 2020-06-01.

Klaus Greff, Rupesh K. Srivastava, Jan Koutník, Bas R. Steunebrink, and Jürgen Schmidhuber.
LSTM: A Search Space Odyssey. *IEEE Trans. Neural Networks Learn. Syst.*, 28(10):2222–2232,
Jul 2016. ISSN 2162-2388. doi: 10.1109/TNNLS.2016.2582924.